Translational regulation enhances distinction of cell types in the nervous system

Authors:

Toshiharu Ichinose[1,2,*], Shu Kondo[3], Mai Kanno[2], Yuichi Shichino[4], Mari Mito[4], Shintaro Iwasaki[4,5], Hiromu Tanimoto[2,*].

Affiliations:

1: Frontier Research Institute for Interdisciplinary Sciences, Tohoku University; 2: Graduate School of Life Sciences, Tohoku University; 3: Faculty of Advanced Engineering, Tokyo University of Sciences; 4: RNA Systems Biochemistry Laboratory, RIKEN Cluster for Pioneering Research, Wako, Saitama 351-0198, Japan 5: Department of Computational Biology and Medical Sciences, Graduate School of Frontier Sciences, The University of Tokyo, Kashiwa, Chiba 277-8561, Japan.

Correspondence authors:

Hiromu Tanimoto (hiromut@m.tohoku.ac.jp) and Toshiharu Ichinose (toshiharu.ichinose.c1@tohoku.ac.jp)

Author Contributions:

TI, SK, and HT conceptualized the project; TI performed ribosome profiling and RNA-seq with the help of YS, MM, and SI; MK performed immunohistochemistry and fluorescent in-situ hybridization, and managed fly care; SK constructed the transgenic reporter strain; YS, MM, and SI contributed to reagents, protocols, and analytic tools; TI analyzed all data with the help of YS and SI; TI and HT wrote the manuscript; SK, YS and SI edited the manuscript.

Competing Interest Statement:

The authors declare no competing interest.

Major Subject Areas:

Neuroscience and Cell Biology

Abstract:

Multicellular organisms are composed of specialized cells with distinct proteomes. While recent advances in single-cell transcriptome analyses have revealed differential expression of mRNAs, cellular diversity in translational profiles remains to be understood. In this study, by performing RNA-seq and ribo-seq in genetically-defined cells in the *Drosophila* brain, we revealed substantial posttranscriptional regulations that augment the cell-type distinctions. Specifically, we found that translational efficiency of proteins fundamental to neuronal functions, such as ion channels and neurotransmitter receptors, was maintained low in glia, leading to preferential translation in neurons. Notably, distribution of ribosome footprints on these mRNAs exhibited a remarkable bias towards the 5′ untranslated regions (UTR) in glia. Using a transgenic reporter, we provide evidence that the UTR confer translational suppression selectively in glia. Overall, these findings underscore the profound impact of translational regulation in shaping cell identity and provide new insights into the molecular mechanisms driving cell-type diversity.

Introduction:

Gene expression is heavily regulated both at the transcription and translation levels (Becker et al., 2018; Casas-Vila et al., 2017; Li et al., 2020; Liu et al., 2016; Schwanhäusser et al., 2011), and its heterogeneity defines the specialized morphologies and functions of cells. The *Drosophila* brain is a well-studied model tissue containing more than 5,000 morphologically distinct cell types (Scheffer et al., 2020). Recent advances in single-cell transcriptomics have identified groups of differentially expressed genes and provided an in-depth overview of cellular diversity in the transcriptomes (Croset et al., 2018; Davie et al., 2018; Li et al., 2022). On the other hand, translational regulations in cell-type specialization remain to be elucidated.

The two major cell types in the brain, neuronal and glial cells, have distinct physiological functions. Neurons are specialized for synaptic and electric communication with high targeted specificity, temporal precision, and long distance. In contrast, glial cells form the blood brain barrier, maintain homeostasis of extracellular ion, nutrition, and neurotransmitters, and act as immune cells (Hartenstein, 2011). Despite these clear differences, the transcriptomes of neurons and glia share similarity according to recent single-cell transcriptome analyses (Croset et al., 2018; Davie et al., 2018; Li et al., 2022), suggesting substantial post-transcriptional processes to distinguish their proteomes.

Ribosome profiling or Ribo-seq, which is based on deep-sequencing of mRNA fragments protected by ribosomes from RNase treatment (ribosome footprints), has been a powerful approach to provide a genome-wide snapshot of protein synthesis ('translatome') (Ingolia et al., 2009). Application of this method, combined with transcriptome analysis, revealed multiple layers of translational regulation in cells. For example, this comparison allowed measurements of translational efficiency (TE), which is quantified as the number of ribosome footprints on the coding sequence per mRNA, and discoveries of previously unannotated ORFs (Dunn et al., 2013; Ingolia et al., 2011, 2009; Zhang et al., 2018). While TE profiles have been reported to be variable among dissected animal tissues (Fujii et al., 2017; Wang et al., 2021; Zhang et al., 2018), differences in translational regulations among identified cell types remain unclear.

Here, we examine the comprehensive landscape of translational profiles between neuronal and glial cells in the *Drosophila* head. Due to the size of the fly brain (~0.5 mm) and intricate intercellular adhesions among neurons and glia (Kremer et al., 2017), surgical separation is impractical. We thus biochemically purified ribosome-bound mRNAs through genetic tagging of ribosomes in target cells (Chen and Dickman, 2017; Sapkota et al., 2019; Scheckel et al., 2020; Thomas et al., 2012; You et al., 2021) and further performed Ribo-seq and RNA-seq. By this comparative transcriptome-translatome analyses, we suggest that differential translational programs enhance the distinction of protein synthesis between neuronal and glial cells.

Results:

Comparative transcriptome-translatome analyses reveal translational suppression of selective groups of proteins in the fly heads

To gain an overview of the translation status, we first applied conventional Ribo-seq in the whole fly head, and successfully monitored footprint distribution at a single-codon resolution (Figure 1A, see 'Materials and Methods' for technical details). The majority (96.2%) of ribosome footprints were mapped onto the annotated coding sequences (CDS), and its distribution displayed a clear 3-nt periodicity, reflecting the codon-wise movement (Figure 1B).

To compare transcriptome and translatome, we also performed RNA-seq from the same lysate (Figure 1A). As previously reported, the transcript level and the number of ribosome footprints did not always match, suggesting substantial post-transcriptional regulations (R^2 = 0.664; Figure 1C). For instance, while *Shaker* (*Sh*) and *Trehalase* (*Treh*), which encode a voltage-gated K^+ channel and an enzyme that hydrolyzes trehalose, respectively, were similar

94 regarding transcript levels, far more ribosome footprints were detected on *Treh* (Figure 1D-E).
95 We therefore measured translational efficiency (TE), ribosome footprints normalized by mRNA
96 reads. TE was much higher for *Treh* than *Sh* (Figure 1F), and we found a striking genome-
97 wide variability with more than 20-fold TE difference between the 5 and 95 percentiles (Figure
98 1G). Kyoto Encyclopedia of Genes and Genome (KEGG) pathway enrichment analysis
99 revealed that transcripts involved in fatty acid metabolism and proteasome are actively
100 translated (Figure 1H). In contrast, ribosome proteins, as previously reported (Chen and
101 Dickman, 2017; Cho et al., 2015), and proteins mediating neuronal ligand-receptor interactions
102 were significantly enriched in the transcripts with low TE, suggesting translational suppression
103 (Figure 1H). Indeed, many transcripts encoding ligand- or voltage-gated ion channels, G-
104 protein coupled receptors (GPCR) showed remarkably low TE (Figure 1C and 1I). These
105 results suggest translational regulations specific to neuronal transcripts in the fly head.

106 **Translational regulation enhances the difference of the gene expression profiles**
107 **between cell types**

108 Because the translatome/transcriptome status of the whole heads was a mixed average
109 of diverse cell types, such as neurons, glial cells, fat bodies, and muscles, we set up an
110 experimental approach to dissect cell-type specific translational regulations. By expressing
111 epitope-tagged RpL3 (uL3 in universal nomenclature) (Chen and Dickman, 2017) under the
112 control of UAS using the *nSyb*- or the *repo*- GAL4 drivers, we immunopurified the tagged
113 ribosomes and associated mRNAs separately from neurons and glia, and performed Ribo-seq
114 (Figure 2A). By immunohistochemistry, we confirmed that *UAS-RpL3::FLAG* on the third
115 chromosome exhibited minimum leakage expression in the brain and did not display any
116 apparent morphological defects upon expression using either driver, compared to other
117 insertions or constructs (Chen and Dickman, 2017; Huang et al., 2019; Thomas et al., 2012)
118 (Figures 2A and Figure 2 – figure supplement 1A-B). By the purification of FLAG-tagged
119 ribosomes, we successfully profiled translatome from neurons and glial cells in the fly heads:
120 Footprints were found on 10,821 (78.4 % of all the annotated genes) and 10,994 (79.7 %)
121 genes in neurons and glia, respectively, with decent reproducibility among the biological
122 replicates (R^2 > 0.9, Figure 2 – figure supplement 1C). The known marker genes were strongly
123 enriched while non-target markers were depleted (Figures 2B and Figure 2 – figure
124 supplement 1D-E) (Croset et al., 2018; Davie et al., 2018; Li et al., 2022), and the KEGG
125 enrichment analysis showed significant enrichment of footprints on genes associated with the
126 known functions of these cell types (Figure 2 – figure supplement 1F). Interestingly, the KEGG
127 analysis also revealed that neurons exhibit a greater extent of protein synthesis related to

128 oxidative phosphorylation and mitochondrial ribosome proteins, while glial cells show higher
129 expression of proteins associated with glycolysis (Figure 2 – figure supplement 1F-G). These
130 findings support the glia-neuron lactate shuttle hypothesis, a recently proposed concept of
131 metabolic specialization (Mason, 2017; Volkenhoff et al., 2015). Furthermore, apart from the
132 annotated CDS, we detected clustered ribosome footprints on *Hsr-ω*, previously annotated as
133 a long non-coding RNA, strongly suggesting the synthesis of hitherto undescribed
134 polypeptides (Figure 2 – figure supplement 1H) (Singh, 2022). Altogether, the combination of
135 genetic labelling of ribosomes in selective cell types and Ribo-seq revealed the differential
136 translatome profiles in the fly heads.

137 To further examine translational regulation, we performed RNA-seq from the same
138 immunoprecipitated lysates (Figures 2A and Figure 2 – figure supplement 2A-B) and
139 calculated TE in neuronal and glial cells. Because our approach relies on the ribosome-mRNA
140 complex, we may miss mRNA with little translational activity, potentially leading to
141 underestimation for such transcripts. Nevertheless, we identified groups of genes undergoing
142 neuron- or glia- specific translational regulations compared to the whole heads (Figure 2 –
143 figure supplement 3A). Genes mediating fatty acid metabolism and degradation, for example,
144 were actively translated in the whole head, but showed lower TE in neurons or in glia (Figures
145 1H and 2C). Because many of these genes are highly expressed in the fat bodies (Chintapalli
146 et al., 2007; Dobson et al., 2018), these results suggest selective translational enhancement
147 in the fat body. Strikingly, TE of genes involved in neuroactive ligand-receptor interaction was
148 significantly higher in neurons but lower in glia (Figure 2C-D), suggesting cell-type specific
149 translational regulation of these genes.

150 This differential translational regulation was highlighted in weak TE correlation between
151 neurons and glia (R^2 = 0.534, Figure 2E). We found that genes transcribed less in glia tend to
152 be further suppressed at translation (Figure 2F). Specifically, many functionally-characterized
153 neuronal genes, such as voltage- or ligand- gated ion channels, G-protein coupled receptors,
154 neuropeptides and proteins for visual perception, showed particularly lower TE in glia (Figures
155 2E, 2G and Figure 2 – figure supplement 3B). For these genes, the distinction between
156 neuronal and glial cells was much exaggerated at the level of translation than at transcription
157 (Figure 2H). Consistently on the genome-wide sacle, the inter-cell type correlation was weaker
158 in translatome compared to in transcriptome (R^2 = 0.59 vs. 0.81, Figure 2 – figure supplement
159 3B). These data together indicate substantial contributions of translational regulation to
160 shaping the cell-type identities.

161 **Biased distribution of ribosomes to upstream open reading frames of neural genes in**
162 **glial cells**

163 We next analyzed the distribution of ribosome footprints on the differentially translated
164 transcripts (DTT). Fat-body related genes showed lower TE in neurons compared to the whole
165 head (Figure 2C). Among these genes, we found a remarkable ribosome accumulation on the
166 start codon specifically in neurons (Figure 3 – figure supplement 1), as if the first round of the
167 elongation cycle was arrested in neurons. On the other hand, DTTs suppressed in glial cells
168 compared to neurons (defined as genes with more than 10 times higher TE in neurons than in
169 glia, n = 161), we noticed that glial ribosome footprints were remarkably biased towards 5′
170 UTR (Figure 3A-B). Notably, this pattern was not obvious on the genome-wide scale (Figure
171 3A-B). The high 5′UTR/CDS ratio of ribosome footprints in glia was commonly observed on
172 many transcripts with known neuronal functions, such as *Rab3, Syt4, Arr1* and *Syn* (Figure
173 3D-E). These results suggest that glial cells suppress the synthesis of neuronal proteins by
174 shifting the ribosome affinity to the 5′ UTR.

175 We reasoned translational downregulation via upstream open reading frames (uORFs) in
176 the 5′ UTR, as the translation of uORFs was reported to suppress that of the downstream main
177 ORF (Ferreira et al., 2013; Zhang et al., 2019, 2018). Consistent with this idea, metagene plot
178 around the AUG codons on 5′ UTR in glia revealed strong accumulation of footprints on the
179 upstream AUG codons, similar to those observed on the initiation codon of CDSs (Figures 4A-
180 B). We calculated the footprint accumulation score on each codon (defined as the ratio of
181 footprints on each codon with surrounding -50/+50 nt), and found that AUG and the near
182 cognate codons (NUG or AUN) showed relatively high accumulation (Figure 4C). On the other
183 hand, any codons did not exhibit the significant accumulation inside the annotated CDS
184 (Figures 4D). Consistently, we found that transcripts related to neuronal functions typically
185 contain long 5′ UTR and many upstream AUG (Figure 4 – figure supplement 1). We thus
186 propose that glial cells suppress the translation of neuronal transcripts by stalling ribosomes
187 on 5′ UTR via uORF.

188 ***Rh1* UTR confers translational suppression in glia**

189 We next asked if the UTR sequences of neuronal genes cause cell-type differences in
190 translation. To this end, we focused on *Rh1* (*Rhodopsin 1*, also known as *ninaE*). The Rh1
191 protein, the opsin with a broadband spectral sensitivity, is heavily expressed in the
192 photoreceptor neurons, and is also responsible for detecting stimuli of other sensory modalities
193 (Leung et al., 2020; O'Tousa et al., 1985; Shen et al., 2011; Zuker et al., 1985). Accordingly,

194 TE of *Rh1* in neurons was 13.5 times as high as that in glial cells (Figure 2 – figure supplement
195 3B). Ribosome footprints on the *Rh1* transcript were heavily biased to 5′ UTR in glia, with the
196 striking accumulation on the putative uORFs composed only of the start and stop codons
197 (Figure 5A).

198 We constructed a transgenic reporter strain using the *Rh1* UTR sequences under the
199 control of UAS (Figure 5B), and directed gene expression ubiquitously using *Tub-GAL4*. The
200 reporter mRNA was detected both in neurons and glial cells. On the other hand, the protein
201 levels were much more heterogeneous and strikingly weak in glia than in neurons (Figure 5C).
202 Driving the reporter expression using the *nSyb*- or *repo-GAL4* driver further corroborated cell-
203 type specific suppression in glia (Figure 5 – figure supplement 1). This post-transcriptional
204 difference between the cell types was in stark contrast to the control reporter strain (DeLuca
205 and Spradling, 2018), which were expressed both in neurons and in glia (Figure 5C). Based
206 on these results, we propose that glial cells selectively suppress the protein synthesis of
207 neuronal genes through the UTR sequence and thereby enhance the translatome distinction
208 from neurons.

209

210 **Discussion:**

211 The comparative translatome-transcriptome analyses in the whole heads, neurons and
212 glial cells revealed the significant diversity of translational regulations across different cell
213 types. Particularly noteworthy was the differential translation of transcripts encoding neuronal
214 proteins, including ion channels and neurotransmitter receptors (Figure 2). These transcripts
215 exhibited preferential translation in neurons (Figure 2), and the relatively long 5′ UTR of these
216 transcripts strongly stalled ribosomes in glia (Figures 3, 4 and Figure 4 – figure supplement 1).
217 While the 5′ UTR-mediated translational regulations are known to be critical for quick response
218 to environmental changes, such as starvation or oxidative stress (Harding et al., 2003; Mueller
219 and Hinnebusch, 1986; Young and Wek, 2016), our study sheds light on its roles in contrasting
220 protein expression among cell types. Furthermore, considering a pivotal role of *de novo* protein
221 synthesis for long-lasting adaptation (Flexner et al., 1963; Tully et al., 1994), it is plausible that
222 similar mechanisms are employed for neuronal plasticity as well. Since several proteins, such
223 as eIF1, MCT-1/DENR, eIF3, and eIF2α kinases, were reported to regulate the rate of
224 translation of uORF or re-initiation after uORFs (Ivanov et al., 2010; Schleich et al., 2014;
225 Sonenberg and Hinnebusch, 2009; Vattem and Wek, 2004), similar molecular machineries
226 might also be recruited for the cell-type distinctions at translation. Given that long 5′ UTRs
227 containing numerous uORFs are also a characteristic feature of neuronal transcripts in

228 mammals (Glock et al., 2021), it is likely that these regulatory mechanisms are evolutionarily
229 conserved.

230 Our cell-type specific translatome analysis further revealed translational regulations
231 beyond 5′ UTR. We found a remarkable ribosomal stall at the initiation codon in several
232 transcripts, a phenomenon observed in neurons but not in the entire heads (Figure 3 – figure
233 supplement 1). These transcripts are known to be massively expressed in the fat bodies but
234 less in the nervous system (Chintapalli et al., 2007; Dobson et al., 2018), and the translation
235 was further suppressed in neurons (Figure 3 – figure supplement 1). Therefore, transition from
236 initiation to elongation may serve as another regulatory checkpoint of protein synthesis
237 (Harnett et al., 2022; Wang et al., 2019), which enhances cell-type distinctions. Furthermore,
238 we found ribosome footprints also on the 3′ UTR of certain transcripts, such as *Synapsin*
239 (Figure 3C). Stop-codon readthrough has been reported to be more frequent in neurons than
240 in other cell types (Hudson et al., 2021; Karki et al., 2022; Prieto-Godino et al., 2016). Because
241 the readthrough events extend the protein C-terminus, its regulation can add yet another layer
242 of cell-type diversity (Dunn et al., 2013; Jungreis et al., 2011; Klagges et al., 1996). Altogether,
243 we here propose that translational regulations further differentiate transcriptome distinctions,
244 thereby shaping the cellular identity.

245 Due to the specialized functions of neuronal and glial cells, they express distinct sets of
246 proteins. Neurons allocate more ribosomes to proteins related to neurotransmission, visual
247 sensing and oxidative phosphorylation, while glial cells synthesize transporters and enzymes
248 for metabolism of amino acid, fatty acid or carbohydrates (Figure 2 – figure supplement 1F).
249 Despite these clear differences and specialization, a significant amount of neuronal and glial
250 cells has a common developmental origin. They originate from a stem cell lineage known as
251 neuro-glioblasts (Lai and Lee, 2006; Viktorin et al., 2011), and the fate of these cells can be
252 altered by the expression of a single gene, *glial cells missing* (*gcm*) (Hartenstein, 2011; Hosoya
253 et al., 1995). Therefore, translational regulations may play a particularly important role in these
254 sister cell types with distinct physiological roles.

255 In the *Drosophila* brain, approximately 100 stem cell lineages diverge into more than
256 5,000 morphologically distinct cell types (Ito et al., 2013; Scheffer et al., 2020; Yu et al., 2013).
257 Hence, translational regulations similar to those described in this study, or other possible
258 regulations, may play significant roles in further differentiating neuronal or glial subtypes.
259 Consistent with this idea, our *UAS-Rh1-Venus* reporter showed heterogeneous expression
260 even among neurons (Figures 5C and Figure 5 – figure supplement 1). Similarly, choline

261 acetyltransferase (ChAT), an enzyme needed to synthesize acetylcholine, is transcribed in
262 many glutamatergic and GABAergic neurons but its protein synthesis is inhibited at the level
263 of translation (Lacin et al., 2019). Altogether, comparative translatome in diverse cell types
264 using more specific GAL4 drivers should highlight the diversity of post-transcriptional
265 regulations leveraged in the brain.

266

267 **Materials and Methods:**

268 **Fly culture and genetics**

269 The flies were reared in a mass culture at 24 ºC under the 12-12 hour light-dark cycles on
270 the standard cornmeal food. The *Canton-S* strain was used as the wild-type. We utilized the
271 following transgenic strains: *w^{1118};;GMR57C10-GAL4* (*nSyb-GAL4*; BDSC #39171),
272 *w^{1118};;repo-GAL4* (BDSC #7415), *y^1w^{1118};;tublin-GAL4* (BDSC #5138), *w^{1118};;UAS-*
273 *RpL3::FLAG* (BDSC #77132) (Chen and Dickman, 2017), *y^1v^1;UAS-Rh1-Venus* (made in this
274 study; see below), *w;UASz-GFP* (a kind gift from Dr. Steven DeLuca) (DeLuca and Spradling,
275 2018). Females of the GAL4 drivers were crossed to males of the UAS effectors, and the F1
276 progenies were used for the experiments. Of note, although *UAS-EGFP::RpL10Ab* (Thomas
277 et al., 2012) has been used to isolate ribosomes from specific cells, its expression using the
278 *repo-GAL4* caused lethality in our hands.

279 **Library preparation for ribosome profiling**

280 *Tissue collection and lysate preparation*

281 Four to eight days old flies with mixed gender were flash-frozen with liquid nitrogen,
282 thoroughly vortexed, and the heads were isolated from the bodies with metal mesh in a similar
283 manner reported previously (Sun et al., 2020). Approximately 500 frozen heads were mixed
284 with 400 µl of frozen droplets of lysis buffer [20 mM Tris-HCl pH7.5, 150mM NaCl, 5 mM $MgCl_2$,
285 1 mM dithiothreitol, 1 % Triton X-100, 100 µg/ml chloramphenicol, and 100 µg/ml
286 cycloheximide] in a pre-chilled container, then pulverized with grinding at 3,000 rpm for 15
287 seconds using a Multi-beads Shocker (YASUI KIKAI). The lysate was slowly thawed at 4 °C
288 and the supernatant was recovered after spinning down by a table top micro centrifuge. The
289 lysate was treated with 10 U of Turbo DNase (ThermoFisher Scientific) on ice for 10 min to
290 digest the genome DNA. The supernatant was further clarified by spinning at 20,000 g for 10
291 minutes.

292 *Immunoprecipitation*

293 Anti-FLAG M2 antibody (F1804, Sigma Aldrich) and Dynabeads M-280 bound to anti-
294 mouse IgG antibody (11201D, Invitrogen) were used for immunoprecipitation. 25 µl of the
295 beads solution, washed twice with the aforementioned lysis buffer, was mixed with 2.5 µl of
296 the M2 antibody, and incubated at 4 °C for 1 hour with rotation. Beads were incubated with the
297 lysate at 4 °C for 1 hour with rotation and washed for four times with the lysis buffer. The

298 ribosome-bound mRNA was eluted with 50 µl of 100 µg/ml 3× FLAG peptide (GEN-3XFLAG-
299 25, Protein Ark) dissolved in the lysis buffer.

300 *RNase digestion and library preparation*

301 Ribosome footprinting was performed as described previously (McGlincy and Ingolia,
302 2017; Mito et al., 2020) with modifications. We used RNase I from *E. coli* (N6901K, Epicentre)
303 to digest the crude (Figures 1, Figure 2 – figure supplement 1C-D) or the immunoprecipitated
304 (Figure 2) lysate. Concentration of RNA in lysate were measured with Qubit RNA HS kit
305 (Q32852, Thermo Fisher Scientific). RNase I was added at a dose of 0.25 U per 1 µg RNA in
306 a 50 µl reaction and incubated at 25 °C for 45 minutes. We used 1.36 µg and 0.5 µg RNA to
307 prepare the whole head libraries (Figures 1, Figure 2 – figure supplement 1C-D) and the cell-
308 type specific libraries (Figure 2-3), respectively. The RNase digestion was stopped by adding
309 20 U of SUPERase•In (AM2694, ThermoFisher Scientific). Ribosomes were isolated by
310 MicroSpin S-400 HR columns (27-5140-01, GE Healthcare). Subsequently, we purified RNA
311 using the TRIzol-LS (10296010, ThermoFisher Scientific) and Direct-zol RNA Microprep kit
312 (R2062, Zymo Research), and isolated the RNA fragment ranging 17 to 34 nt by
313 polyacrylamide gel electrophoresis.

314 The isolated RNA fragments were ligated to custom-made preadenylated linkers
315 containing unique molecular identifiers and barcodes for library pooling, using T4 RNA ligase
316 2, truncated KQ (M0373L, New England Biolabs) (Mito et al., 2020). Ribosomal RNA was
317 depleted by hybridizing to the custom-made biotinylated 2′-*O*-methyl oligonucleotides with
318 complementary sequences to the *Drosophila* rRNA (see *Supplementary Method* for the
319 sequences), which can be pulled-down using the streptavidin-coated beads (65001,
320 ThermoFisher Scientific). The rRNA-depleted samples were reverse-transcribed with
321 ProtoScript II (M0368L, New England Biolabs), circularized with CircLigase II (CL9025K,
322 Epicentre), and PCR-amplified using Phusion polymerase (M0530S, New England Biolabs)
323 (Mito et al., 2020). The libraries were sequenced with the Illumina HiSeq 4000 system
324 (Illumina) with an option of single end reads for 50 bases.

325 **Library preparation for transcriptome analysis**

326 The crude (Figure 1) or the immunoprecipitated (Figure 2) lysate was prepared using the
327 same protocol as described above, but without RNase digestion. RNA was purified using
328 TRIzol-LS. The libraries were constructed in Azenta Japan Corporation, using the NEBNext
329 Poly(A) mRNA Magnetic Isolation Module (E7760, New England Biolabs) and MGIEasy RNA
330 Directional Library Prep kit (1000006386, MGI tech). Briefly, poly-A tailed mRNAs were

331 enriched with the oligo dT beads, fragmented, and reverse-transcribed using random primers.
332 After the second strand cDNA was synthesized, an adapter sequence was added. DNA library
333 was PCR-amplified. The libraries were sequenced with DNB-seq (MGI tech) with an option of
334 paired end reads for 150 bases.

335 **Data analysis**

336 Adaptor sequences were removed using Fastp (Chen et al., 2018), and the reads that
337 matched to the non-coding RNA were discarded. The remaining reads were mapped onto the
338 *Drosophila melanogaster* release 6 genome. Mapping was performed using STAR (Dobin et
339 al., 2013). PCR-duplicated reads were removed by referring to the unique molecular identifiers.
340 The number of uniquely mapped reads are as follows:

341 Ribo-seq:

Sample	#Reads
Canton-S, whole heads	1,427,090
nSyb-GAL4/UAS-RpL3::FLAG, after IP, replicate 1	2,443,467
nSyb-GAL4/UAS-RpL3::FLAG, after IP, replicate 2	1,135,284
repo-GAL4/UAS-RpL3::FLAG, after IP, replicate 1	2,698,259
repo-GAL4/UAS-RpL3::FLAG, after IP, replicate 2	2,133,920
nSyb-GAL4/UAS-RpL3::FLAG, whole heads, replicate 1	2,147,092
nSyb-GAL4/UAS-RpL3::FLAG, whole heads, replicate 2	2,361,588
repo-GAL4/UAS-RpL3::FLAG, whole heads, replicate 1	1,372,502
repo-GAL4/UAS-RpL3::FLAG, whole heads, replicate 2	1,846,122

342

343 RNA-seq:

Sample	#Reads
Canton-S, whole heads	29,132,939
nSyb-GAL4/UAS-RpL3::FLAG, after IP, replicate 1	40,638,850
nSyb-GAL4/UAS-RpL3::FLAG, after IP, replicate 2	34,247,848
repo-GAL4/UAS-RpL3::FLAG, after IP, replicate 1	30,906,375
repo-GAL4/UAS-RpL3::FLAG, after IP, replicate 2	31,928,337

344

345 For Ribo-seq analysis, fragments ranging from 20 to 34 nt for whole head samples and
346 21 to 36 nt for immunoprecipitated samples were used. For the whole head samples, the
347 position of the P site was estimated as 12 or 13 nt downstream from the 5′ end, for the 20 to
348 31 nt or 32-34 nt fragments, respectively (Ingolia et al., 2009). For the immunoprecipitated
349 samples, it was estimated as 12 or 13 nt downstream for the 21 nt or 22-36 nt fragments,
350 respectively. Footprints were considered to be on the CDS if the estimated P site was between
351 the annotated start and stop codons. RNA-seq analysis included all fragments greater than 30
352 nt in length. For genes with alternatively spliced transcripts, the isoform with the highest TPM
353 in the wild type RNA-seq sample (Figure 1) was selected as the 'representative' isoform. If not
354 specified, only the representative isoforms were considered. TE was calculated as TPM of
355 ribosome footprints on CDS divided by TPM of RNA-seq.

356 The KEGG-enrichment analyses were performed using iPAGE (Figures 1H and 2D)
357 (Goodarzi et al., 2009) or DAVID (Figure 2 – figure supplement 1F and Figure 2 – figure
358 supplement 3A) (Dennis et al., 2003). Statistical tests were performed with GraphPad Prism
359 9.

360 **Reporter construct and the transgenic strain**

361 A DNA fragment containing a minimal hsp70 promoter (hsp70Bb) (DeLuca and Spradling,
362 2018), the 5′ UTR and the first 15 bases of the CDS of *Rh1-RA*, the Venus yellow fluorescent
363 protein gene, and the 3′ UTR of *Rh1-RA* was synthesized and cloned into the pBFv-UAS3
364 plasmid (Addgene #138399). The sequence of the resultant plasmid is provided in the
365 *Supporting Information Text*. The plasmid was then injected into y^1 v^1 *P{nos-phiC31};*
366 *P{CaryP}attP40,* and their progenies were screened for a *v+* phenotype. A single transformant
367 was crossed to y^1 cho^2 v^1*; Sp/CyO* balancer to establish a transgenic line.

368 **Immunohistochemistry and fluorescent in-situ hybridization**

369 Immunohistochemistry (Figures 2A and Figure 2 – figure supplement 1A-B) was
370 performed as previously described with minor modifications (Kanno et al., 2021). Briefly,
371 dissected male fly brains were fixed in 2 % paraformaldehyde in PBS for 1 hour at room
372 temperature, washed three times with PBST (0.1 % Triton X-100 in PBS), blocked with 3 %
373 goat serum in PBST for 30 minutes, then incubated with the primary antibody solution at 4 ºC
374 overnight (mouse anti-FLAG (1:1000; Sigma-Aldrich; F1804) and rat anti-elav (1:20; DSHB;
375 7E8A10)). Subsequently, the brains were washed for three times with PBST, incubated with

376 the secondary antibody solution at 4 ºC overnight (anti-mouse Alexa Fluor 488 (1:400;
377 Invitrogen; A11001) and anti-rat Cy3 (1:200; Jackson ImmunoResearch; 112-166-003)),
378 washed three times with PBST and mounted with 86 % glycerol in PBS.

379 Fluorescent in-situ hybridization, combined with immunohistochemistry, was performed in
380 a similar manner to (Yang et al., 2017) with several modifications (Figure 5C). Dissected male
381 fly brains were fixed in PBS containing 3 % formaldehyde, 1 % glyoxal and 0.1 % methanol for
382 30 min at room temperature, followed by three quick washes with PBT (0.5 % Triton X-100 in
383 PBS). Consistent with the previous study, addition of glyoxal to the fixative improved the FISH
384 signal (Yao et al., 2021). The buffer was then exchanged to the wash solution (10 % Hi-Di™
385 Formamide (Thermofisher scientific; 4311320) in 2x saline sodium citrate (SSC)) and was
386 incubated at 37 ºC for 5 minutes. Subsequently, the brains were incubated with the custom-
387 made Stellaris *Venus* or *GFP* probes (100 nM; see *Supporting Information Text* for the
388 sequences; LGC BioSearch Technologies) and the primary antibody (mouse anti-Repo (1:100;
389 DSHB; 8D12)) in the hybridization buffer (10% Hi-Di™ Formamide in hybridization buffer
390 (Stellaris RNA FISH Hybridization Buffer, SMF-HB1-10)) at 37 ºC for 16 hours. The probes
391 and the antibody were then removed by washing the samples quickly three times with
392 preheated wash solution at 37 ºC, followed by three washes for 10 minutes at room
393 temperature. Blocking was performed with 3 % normal goat serum in PBT for 30 min at room
394 temperature. The secondary antibody (Cy3 goat anti-mouse (1:2000; Jackson
395 ImmunoResearch; 115-166-003)) was then added and was incubated at 4 ºC overnight. The
396 samples were washed once quickly, three times for 20 minutes, and once for 60 minutes with
397 PBT, and then mounted in 86 % glycerol in 1x Tris-HCl buffer (pH7.4).

398 Tissues to detect native GFP or Venus signals (Figure 5 – figure supplement 1) were
399 prepared as follows: dissected brains were fixed in PBS containing 3 % formaldehyde, 1 %
400 glyoxal and 0.1 % methanol for 30 min at room temperature, followed by one quick wash and
401 three washes for 10 minutes with PBT. The samples were then mounted in 86 % glycerol in
402 1x Tris-HCl buffer (pH7.4).

403 **Imaging and microscopes**

404 Imaging was done on the Olympus FV1200 confocal microscope with GaAsP sensors. A
405 100x/1.35 silicone immersion objective (UPLSAPO100XS, Olympus) or 30x/1.05 silicone
406 immersion objective (UPLSAPO30XS) was used. Scan settings were kept constant across
407 specimens to be compared.

Acknowledgments:

We thank Dr. Steven DeLuca (Brandeis university), Dr. Atsushi Sugie (Niigata University), and Dr. Yohei Nitta (Niigata University) for kindly providing the transgenic flies. We also thank Dr. Yusuke Kimura and Dr. Yukihide Tomari (The University of Tokyo) for designing the fly rRNA-depletion probes, Ayako Abe (Tohoku University) for technical assistance, Dr. Takashi Makino (Tohoku University) for critical discussion, Madoka Ichinose for critical comments on the graphic design, and the HOKUSAI SailingShip supercomputer facility at RIKEN for computational supports.

This study was supported by the Ministry of Education, Culture, Sports, Science and Technology (MEXT): 21K06369 (to TI), 21H05713 (to TI), JP20H05784 (to SI), JP21K15023 (to YS), 22H05481 (to HT), 22KK0106 (to HT), 20H00519 (to HT); Japan Society for the Promotion of Science (JSPS): 21K06369 (to TI), JP21K15023 (to YS); Japan Agency for Medical Research and Development (AMED): JP23gm1410001 (to SI); Takeda Life Science Research Grant (to TI); RIKEN-Tohoku Univ Science & Technology Hub Collaborative Research Program (to TI and YS), “Biology of Intracellular Environments” (to SI), Special Postdoctoral Researchers (to YS), and Incentive Research Projects (to YS), Tohoku University Research Program “Frontier Research in Duo” (to HT).

427 **References:**

428 Becker, K., Bluhm, A., Casas-Vila, N., Dinges, N., Dejung, M., Sayols, S., Kreutz, C., Roignant,
429 J.-Y., Butter, F., Legewie, S., 2018. Quantifying post-transcriptional regulation in the
430 development of Drosophila melanogaster. Nat Commun 9, 4970.
431 https://doi.org/10.1038/s41467-018-07455-9
432 Casas-Vila, N., Bluhm, A., Sayols, S., Dinges, N., Dejung, M., Altenhein, T., Kappei, D.,
433 Altenhein, B., Roignant, J.-Y., Butter, F., 2017. The developmental proteome of
434 *Drosophila melanogaster*. Genome Res. 27, 1273–1285.
435 https://doi.org/10.1101/gr.213694.116
436 Chen, S., Zhou, Y., Chen, Y., Gu, J., 2018. fastp: an ultra-fast all-in-one FASTQ preprocessor.
437 Bioinformatics 34, i884–i890. https://doi.org/10.1093/bioinformatics/bty560
438 Chen, X., Dickman, D., 2017. Development of a tissue-specific ribosome profiling approach in
439 Drosophila enables genome-wide evaluation of translational adaptations. PLoS Genet
440 13, e1007117. https://doi.org/10.1371/journal.pgen.1007117
441 Chintapalli, V.R., Wang, J., Dow, J.A.T., 2007. Using FlyAtlas to identify better Drosophila
442 melanogaster models of human disease. Nat Genet 39, 715–720.
443 https://doi.org/10.1038/ng2049
444 Cho, J., Yu, N.-K., Choi, J.-H., Sim, S.-E., Kang, S.J., Kwak, C., Lee, S.-W., Kim, J., Choi, D.I.,
445 Kim, V.N., Kaang, B.-K., 2015. Multiple repressive mechanisms in the hippocampus
446 during memory formation. Science 350, 82–87.
447 https://doi.org/10.1126/science.aac7368
448 Croset, V., Treiber, C.D., Waddell, S., 2018. Cellular diversity in the Drosophila midbrain
449 revealed by single-cell transcriptomics. eLife 7, e34550.
450 https://doi.org/10.7554/eLife.34550
451 Davie, K., Janssens, J., Koldere, D., De Waegeneer, M., Pech, U., Kreft, Ł., Aibar, S.,
452 Makhzami, S., Christiaens, V., Bravo González-Blas, C., Poovathingal, S., Hulselmans,
453 G., Spanier, K.I., Moerman, T., Vanspauwen, B., Geurs, S., Voet, T., Lammertyn, J.,
454 Thienpont, B., Liu, S., Konstantinides, N., Fiers, M., Verstreken, P., Aerts, S., 2018. A
455 Single-Cell Transcriptome Atlas of the Aging Drosophila Brain. Cell 174, 982-998.e20.
456 https://doi.org/10.1016/j.cell.2018.05.057
457 DeLuca, S.Z., Spradling, A.C., 2018. Efficient Expression of Genes in the *Drosophila* Germline
458 Using a UAS Promoter Free of Interference by Hsp70 piRNAs. Genetics 209, 381–
459 387. https://doi.org/10.1534/genetics.118.300874
460 Dennis, G., Sherman, B.T., Hosack, D.A., Yang, J., Gao, W., Lane, H.C., Lempicki, R.A., 2003.
461 DAVID: Database for Annotation, Visualization, and Integrated Discovery. Genome
462 Biol 4, R60. https://doi.org/10.1186/gb-2003-4-9-r60
463 Dobin, A., Davis, C.A., Schlesinger, F., Drenkow, J., Zaleski, C., Jha, S., Batut, P., Chaisson,
464 M., Gingeras, T.R., 2013. STAR: ultrafast universal RNA-seq aligner. Bioinformatics
465 29, 15–21. https://doi.org/10.1093/bioinformatics/bts635
466 Dobson, A.J., He, X., Blanc, E., Bolukbasi, E., Feseha, Y., Yang, M., Piper, M.D.W., 2018.
467 Tissue-specific transcriptome profiling of Drosophila reveals roles for GATA
468 transcription factors in longevity by dietary restriction. npj Aging Mech Dis 4, 5.
469 https://doi.org/10.1038/s41514-018-0024-4
470 Dunn, J.G., Foo, C.K., Belletier, N.G., Gavis, E.R., Weissman, J.S., 2013. Ribosome profiling
471 reveals pervasive and regulated stop codon readthrough in Drosophila melanogaster.
472 eLife 2, e01179. https://doi.org/10.7554/eLife.01179
473 Ferreira, J.P., Overton, K.W., Wang, C.L., 2013. Tuning gene expression with synthetic
474 upstream open reading frames. Proc. Natl. Acad. Sci. U.S.A. 110, 11284–11289.
475 https://doi.org/10.1073/pnas.1305590110

476 Flexner, J.B., Flexner, L.B., Stellar, E., 1963. Memory in mice as affected by intracerebral
477 puromycin. Science 141, 57–59. https://doi.org/10.1126/science.141.3575.57
478 Fujii, K., Shi, Z., Zhulyn, O., Denans, N., Barna, M., 2017. Pervasive translational regulation
479 of the cell signalling circuitry underlies mammalian development. Nat Commun 8,
480 14443. https://doi.org/10.1038/ncomms14443
481 Glock, C., Biever, A., Tushev, G., Nassim-Assir, B., Kao, A., Bartnik, I., tom Dieck, S.,
482 Schuman, E.M., 2021. The translatome of neuronal cell bodies, dendrites, and axons.
483 Proc. Natl. Acad. Sci. U.S.A. 118, e2113929118.
484 https://doi.org/10.1073/pnas.2113929118
485 Goodarzi, H., Elemento, O., Tavazoie, S., 2009. Revealing Global Regulatory Perturbations
486 across Human Cancers. Molecular Cell 36, 900–911.
487 https://doi.org/10.1016/j.molcel.2009.11.016
488 Harding, H.P., Zhang, Y., Zeng, H., Novoa, I., Lu, P.D., Calfon, M., Sadri, N., Yun, C., Popko,
489 B., Paules, R., Stojdl, D.F., Bell, J.C., Hettmann, T., Leiden, J.M., Ron, D., 2003. An
490 Integrated Stress Response Regulates Amino Acid Metabolism and Resistance to
491 Oxidative Stress. Molecular Cell 11, 619–633. https://doi.org/10.1016/S1097-
492 2765(03)00105-9
493 Harnett, D., Ambrozkiewicz, M.C., Zinnall, U., Rusanova, A., Borisova, E., Drescher, A.N.,
494 Couce-Iglesias, M., Villamil, G., Dannenberg, R., Imami, K., Münster-Wandowski, A.,
495 Fauler, B., Mielke, T., Selbach, M., Landthaler, M., Spahn, C.M.T., Tarabykin, V., Ohler,
496 U., Kraushar, M.L., 2022. A critical period of translational control during brain
497 development at codon resolution. Nat Struct Mol Biol 29, 1277–1290.
498 https://doi.org/10.1038/s41594-022-00882-9
499 Hartenstein, V., 2011. Morphological diversity and development of glia in *Drosophila*. Glia 59,
500 1237–1252. https://doi.org/10.1002/glia.21162
501 Hosoya, T., Takizawa, K., Nitta, K., Hotta, Y., 1995. Glial cells missing: A binary switch
502 between neuronal and glial determination in drosophila. Cell 82, 1025–1036.
503 https://doi.org/10.1016/0092-8674(95)90281-3
504 Huang, K., Chen, W., Zhu, F., Li, P.W.-L., Kapahi, P., Bai, H., 2019. RiboTag translatomic
505 profiling of Drosophila oenocytes under aging and induced oxidative stress. BMC
506 Genomics 20, 50. https://doi.org/10.1186/s12864-018-5404-4
507 Hudson, A.M., Szabo, N.L., Loughran, G., Wills, N.M., Atkins, J.F., Cooley, L., 2021. Tissue-
508 specific dynamic codon redefinition in *Drosophila*. Proc. Natl. Acad. Sci. U.S.A. 118,
509 e2012793118. https://doi.org/10.1073/pnas.2012793118
510 Ingolia, N.T., Ghaemmaghami, S., Newman, J.R.S., Weissman, J.S., 2009. Genome-wide
511 analysis in vivo of translation with nucleotide resolution using ribosome profiling.
512 Science 324, 218–223. https://doi.org/10.1126/science.1168978
513 Ingolia, N.T., Lareau, L.F., Weissman, J.S., 2011. Ribosome Profiling of Mouse Embryonic
514 Stem Cells Reveals the Complexity and Dynamics of Mammalian Proteomes. Cell 147,
515 789–802. https://doi.org/10.1016/j.cell.2011.10.002
516 Ito, M., Masuda, N., Shinomiya, K., Endo, K., Ito, K., 2013. Systematic Analysis of Neural
517 Projections Reveals Clonal Composition of the Drosophila Brain. Current Biology 23,
518 644–655. https://doi.org/10.1016/j.cub.2013.03.015
519 Ivanov, I.P., Loughran, G., Sachs, M.S., Atkins, J.F., 2010. Initiation context modulates
520 autoregulation of eukaryotic translation initiation factor 1 (eIF1). Proc. Natl. Acad. Sci.
521 U.S.A. 107, 18056–18060. https://doi.org/10.1073/pnas.1009269107
522 Jungreis, I., Lin, M.F., Spokony, R., Chan, C.S., Negre, N., Victorsen, A., White, K.P., Kellis,
523 M., 2011. Evidence of abundant stop codon readthrough in *Drosophila* and other
524 metazoa. Genome Res. 21, 2096–2113. https://doi.org/10.1101/gr.119974.110

Kanno, M., Hiramatsu, S., Kondo, S., Tanimoto, H., Ichinose, T., 2021. Voluntary intake of psychoactive substances is regulated by the dopamine receptor Dop1R1 in Drosophila. Sci Rep 11, 3432. https://doi.org/10.1038/s41598-021-82813-0

Karki, P., Carney, T.D., Maracci, C., Yatsenko, A.S., Shcherbata, H.R., Rodnina, M.V., 2022. Tissue-specific regulation of translational readthrough tunes functions of the traffic jam transcription factor. Nucleic Acids Research 50, 6001–6019. https://doi.org/10.1093/nar/gkab1189

Klagges, B.R.E., Heimbeck, G., Godenschwege, T.A., Hofbauer, A., Pflugfelder, G.O., Reifegerste, R., Reisch, D., Schaupp, M., Buchner, S., Buchner, E., 1996. Invertebrate Synapsins: A Single Gene Codes for Several Isoforms in *Drosophila*. J. Neurosci. 16, 3154–3165. https://doi.org/10.1523/JNEUROSCI.16-10-03154.1996

Kremer, M.C., Jung, C., Batelli, S., Rubin, G.M., Gaul, U., 2017. The glia of the adult *Drosophila* nervous system: Glia Anatomy in Adult Drosophila Nervous System. Glia 65, 606–638. https://doi.org/10.1002/glia.23115

Lacin, H., Chen, H.-M., Long, X., Singer, R.H., Lee, T., Truman, J.W., 2019. Neurotransmitter identity is acquired in a lineage-restricted manner in the Drosophila CNS. eLife 8, e43701. https://doi.org/10.7554/eLife.43701

Lai, S.-L., Lee, T., 2006. Genetic mosaic with dual binary transcriptional systems in Drosophila. Nat Neurosci 9, 703–709. https://doi.org/10.1038/nn1681

Leung, N.Y., Thakur, D.P., Gurav, A.S., Kim, S.H., Di Pizio, A., Niv, M.Y., Montell, C., 2020. Functions of Opsins in Drosophila Taste. Current Biology 30, 1367-1379.e6. https://doi.org/10.1016/j.cub.2020.01.068

Li, H., Janssens, J., De Waegeneer, M., Kolluru, S.S., Davie, K., Gardeux, V., Saelens, W., David, F.P.A., Brbić, M., Spanier, K., Leskovec, J., McLaughlin, C.N., Xie, Q., Jones, R.C., Brueckner, K., Shim, J., Tattikota, S.G., Schnorrer, F., Rust, K., Nystul, T.G., Carvalho-Santos, Z., Ribeiro, C., Pal, S., Mahadevaraju, S., Przytycka, T.M., Allen, A.M., Goodwin, S.F., Berry, C.W., Fuller, M.T., White-Cooper, H., Matunis, E.L., DiNardo, S., Galenza, A., O'Brien, L.E., Dow, J.A.T., FCA Consortium§, Jasper, H., Oliver, B., Perrimon, N., Deplancke, B., Quake, S.R., Luo, L., Aerts, S., Agarwal, D., Ahmed-Braimah, Y., Arbeitman, M., Ariss, M.M., Augsburger, J., Ayush, K., Baker, C.C., Banisch, T., Birker, K., Bodmer, R., Bolival, B., Brantley, S.E., Brill, J.A., Brown, N.C., Buehner, N.A., Cai, X.T., Cardoso-Figueiredo, R., Casares, F., Chang, A., Clandinin, T.R., Crasta, S., Desplan, C., Detweiler, A.M., Dhakan, D.B., Donà, E., Engert, S., Floc'hlay, S., George, N., González-Segarra, A.J., Groves, A.K., Gumbin, S., Guo, Y., Harris, D.E., Heifetz, Y., Holtz, S.L., Horns, F., Hudry, B., Hung, R.-J., Jan, Y.N., Jaszczak, J.S., Jefferis, G.S.X.E., Karkanias, J., Karr, T.L., Katheder, N.S., Kezos, J., Kim, A.A., Kim, S.K., Kockel, L., Konstantinides, N., Kornberg, T.B., Krause, H.M., Labott, A.T., Laturney, M., Lehmann, R., Leinwand, S., Li, J., Li, J.S.S., Li, Kai, Li, Ke, Li, L., Li, T., Litovchenko, M., Liu, H.-H., Liu, Y., Lu, T.-C., Manning, J., Mase, A., Matera-Vatnick, M., Matias, N.R., McDonough-Goldstein, C.E., McGeever, A., McLachlan, A.D., Moreno-Roman, P., Neff, N., Neville, M., Ngo, S., Nielsen, T., O'Brien, C.E., Osumi-Sutherland, D., Özel, M.N., Papatheodorou, I., Petkovic, M., Pilgrim, C., Pisco, A.O., Reisenman, C., Sanders, E.N., dos Santos, G., Scott, K., Sherlekar, A., Shiu, P., Sims, D., Sit, R.V., Slaidina, M., Smith, H.E., Sterne, G., Su, Y.-H., Sutton, D., Tamayo, M., Tan, M., Tastekin, I., Treiber, C., Vacek, D., Vogler, G., Waddell, S., Wang, W., Wilson, R.I., Wolfner, M.F., Wong, Y.-C.E., Xie, A., Xu, J., Yamamoto, S., Yan, J., Yao, Z., Yoda, K., Zhu, R., Zinzen, R.P., 2022. Fly Cell Atlas: A single-nucleus transcriptomic atlas of the adult fruit fly. Science 375, eabk2432. https://doi.org/10.1126/science.abk2432

Li, J., Han, S., Li, H., Udeshi, N.D., Svinkina, T., Mani, D.R., Xu, C., Guajardo, R., Xie, Q., Li, T., Luginbuhl, D.J., Wu, B., McLaughlin, C.N., Xie, A., Kaewsapsak, P., Quake, S.R.,

576 Carr, S.A., Ting, A.Y., Luo, L., 2020. Cell-Surface Proteomic Profiling in the Fly Brain
577 Uncovers Wiring Regulators. Cell 180, 373-386.e15.
578 https://doi.org/10.1016/j.cell.2019.12.029
579 Liu, Y., Beyer, A., Aebersold, R., 2016. On the Dependency of Cellular Protein Levels on
580 mRNA Abundance. Cell 165, 535–550. https://doi.org/10.1016/j.cell.2016.03.014
581 Mason, S., 2017. Lactate Shuttles in Neuroenergetics—Homeostasis, Allostasis and Beyond.
582 Front. Neurosci. 11. https://doi.org/10.3389/fnins.2017.00043
583 McGlincy, N.J., Ingolia, N.T., 2017. Transcriptome-wide measurement of translation by
584 ribosome profiling. Methods 126, 112–129.
585 https://doi.org/10.1016/j.ymeth.2017.05.028
586 Mito, M., Mishima, Y., Iwasaki, S., 2020. Protocol for Disome Profiling to Survey Ribosome
587 Collision in Humans and Zebrafish. STAR Protocols 1, 100168.
588 https://doi.org/10.1016/j.xpro.2020.100168
589 Mueller, P.P., Hinnebusch, A.G., 1986. Multiple upstream AUG codons mediate translational
590 control of GCN4. Cell 45, 201–207. https://doi.org/10.1016/0092-8674(86)90384-3
591 O'Tousa, J.E., Baehr, W., Martin, R.L., Hirsh, J., Pak, W.L., Applebury, M.L., 1985. The
592 Drosophila ninaE gene encodes an opsin. Cell 40, 839–850.
593 https://doi.org/10.1016/0092-8674(85)90343-5
594 Prieto-Godino, L.L., Rytz, R., Bargeton, B., Abuin, L., Arguello, J.R., Peraro, M.D., Benton, R.,
595 2016. Olfactory receptor pseudo-pseudogenes. Nature 539, 93–97.
596 https://doi.org/10.1038/nature19824
597 Sapkota, D., Lake, A.M., Yang, W., Yang, C., Wesseling, H., Guise, A., Uncu, C., Dalal, J.S.,
598 Kraft, A.W., Lee, J.-M., Sands, M.S., Steen, J.A., Dougherty, J.D., 2019. Cell-Type-
599 Specific Profiling of Alternative Translation Identifies Regulated Protein Isoform
600 Variation in the Mouse Brain. Cell Reports 26, 594-607.e7.
601 https://doi.org/10.1016/j.celrep.2018.12.077
602 Scheckel, C., Imeri, M., Schwarz, P., Aguzzi, A., 2020. Ribosomal profiling during prion
603 disease uncovers progressive translational derangement in glia but not in neurons.
604 eLife 9, e62911. https://doi.org/10.7554/eLife.62911
605 Scheffer, L.K., Xu, C.S., Januszewski, M., Lu, Z., Takemura, Shin-ya, Hayworth, K.J., Huang,
606 G.B., Shinomiya, K., Maitlin-Shepard, J., Berg, S., Clements, J., Hubbard, P.M., Katz,
607 W.T., Umayam, L., Zhao, T., Ackerman, D., Blakely, T., Bogovic, J., Dolafi, T.,
608 Kainmueller, D., Kawase, T., Khairy, K.A., Leavitt, L., Li, P.H., Lindsey, L., Neubarth,
609 N., Olbris, D.J., Otsuna, H., Trautman, E.T., Ito, M., Bates, A.S., Goldammer, J., Wolff,
610 T., Svirskas, R., Schlegel, P., Neace, E., Knecht, C.J., Alvarado, C.X., Bailey, D.A.,
611 Ballinger, S., Borycz, J.A., Canino, B.S., Cheatham, N., Cook, M., Dreher, M., Duclos,
612 O., Eubanks, B., Fairbanks, K., Finley, S., Forknall, N., Francis, A., Hopkins, G.P.,
613 Joyce, E.M., Kim, S., Kirk, N.A., Kovalyak, J., Lauchie, S.A., Lohff, A., Maldonado, C.,
614 Manley, E.A., McLin, S., Mooney, C., Ndama, M., Ogundeyi, O., Okeoma, N., Ordish,
615 C., Padilla, N., Patrick, C.M., Paterson, T., Phillips, E.E., Phillips, E.M., Rampally, N.,
616 Ribeiro, C., Robertson, M.K., Rymer, J.T., Ryan, S.M., Sammons, M., Scott, A.K.,
617 Scott, A.L., Shinomiya, A., Smith, C., Smith, K., Smith, N.L., Sobeski, M.A., Suleiman,
618 A., Swift, J., Takemura, Satoko, Talebi, I., Tarnogorska, D., Tenshaw, E., Tokhi, T.,
619 Walsh, J.J., Yang, T., Horne, J.A., Li, F., Parekh, R., Rivlin, P.K., Jayaraman, V., Costa,
620 M., Jefferis, G.S., Ito, K., Saalfeld, S., George, R., Meinertzhagen, I.A., Rubin, G.M.,
621 Hess, H.F., Jain, V., Plaza, S.M., 2020. A connectome and analysis of the adult
622 Drosophila central brain. eLife 9, e57443. https://doi.org/10.7554/eLife.57443
623 Schleich, S., Strassburger, K., Janiesch, P.C., Koledachkina, T., Miller, K.K., Haneke, K.,
624 Cheng, Y.-S., Küchler, K., Stoecklin, G., Duncan, K.E., Teleman, A.A., 2014. DENR–
625 MCT-1 promotes translation re-initiation downstream of uORFs to control tissue growth.
626 Nature 512, 208–212. https://doi.org/10.1038/nature13401

627 Schwanhäusser, B., Busse, D., Li, N., Dittmar, G., Schuchhardt, J., Wolf, J., Chen, W., Selbach,
628 M., 2011. Global quantification of mammalian gene expression control. Nature 473,
629 337–342. https://doi.org/10.1038/nature10098
630 Shen, W.L., Kwon, Y., Adegbola, A.A., Luo, J., Chess, A., Montell, C., 2011. Function of
631 Rhodopsin in Temperature Discrimination in *Drosophila*. Science 331, 1333–1336.
632 https://doi.org/10.1126/science.1198904
633 Singh, A.K., 2022. Hsrω and Other lncRNAs in Neuronal Functions and Disorders in
634 Drosophila. Life 13, 17. https://doi.org/10.3390/life13010017
635 Sonenberg, N., Hinnebusch, A.G., 2009. Regulation of Translation Initiation in Eukaryotes:
636 Mechanisms and Biological Targets. Cell 136, 731–745.
637 https://doi.org/10.1016/j.cell.2009.01.042
638 Sun, H., Nishioka, T., Hiramatsu, S., Kondo, S., Amano, M., Kaibuchi, K., Ichinose, T.,
639 Tanimoto, H., 2020. Dopamine Receptor Dop1R2 Stabilizes Appetitive Olfactory
640 Memory through the Raf/MAPK Pathway in Drosophila. J. Neurosci. 40, 2935–2942.
641 https://doi.org/10.1523/JNEUROSCI.1572-19.2020
642 Thomas, A., Lee, P.-J., Dalton, J.E., Nomie, K.J., Stoica, L., Costa-Mattioli, M., Chang, P.,
643 Nuzhdin, S., Arbeitman, M.N., Dierick, H.A., 2012. A Versatile Method for Cell-Specific
644 Profiling of Translated mRNAs in Drosophila. PLoS ONE 7, e40276.
645 https://doi.org/10.1371/journal.pone.0040276
646 Tully, T., Preat, T., Boynton, S.C., Del Vecchio, M., 1994. Genetic dissection of consolidated
647 memory in Drosophila. Cell 79, 35–47. https://doi.org/10.1016/0092-8674(94)90398-0
648 Vattem, K.M., Wek, R.C., 2004. Reinitiation involving upstream ORFs regulates *ATF4* mRNA
649 translation in mammalian cells. Proc. Natl. Acad. Sci. U.S.A. 101, 11269–11274.
650 https://doi.org/10.1073/pnas.0400541101
651 Viktorin, G., Riebli, N., Popkova, A., Giangrande, A., Reichert, H., 2011. Multipotent neural
652 stem cells generate glial cells of the central complex through transit amplifying
653 intermediate progenitors in Drosophila brain development. Developmental Biology 356,
654 553–565. https://doi.org/10.1016/j.ydbio.2011.06.013
655 Volkenhoff, A., Weiler, A., Letzel, M., Stehling, M., Klämbt, C., Schirmeier, S., 2015. Glial
656 Glycolysis Is Essential for Neuronal Survival in Drosophila. Cell Metabolism 22, 437–
657 447. https://doi.org/10.1016/j.cmet.2015.07.006
658 Wang, H., Wang, Y., Yang, J., Zhao, Q., Tang, N., Chen, C., Li, H., Cheng, C., Xie, M., Yang,
659 Y., Xie, Z., 2021. Tissue- and stage-specific landscape of the mouse translatome.
660 Nucleic Acids Research 49, 6165–6180. https://doi.org/10.1093/nar/gkab482
661 Wang, J., Johnson, A.G., Lapointe, C.P., Choi, J., Prabhakar, A., Chen, D.-H., Petrov, A.N.,
662 Puglisi, J.D., 2019. eIF5B gates the transition from translation initiation to elongation.
663 Nature 573, 605–608. https://doi.org/10.1038/s41586-019-1561-0
664 Yang, L., Titlow, J., Ennis, D., Smith, C., Mitchell, J., Young, F.L., Waddell, S., Ish-Horowicz,
665 D., Davis, I., 2017. Single molecule fluorescence in situ hybridisation for quantitating
666 post-transcriptional regulation in Drosophila brains. Methods 126, 166–176.
667 https://doi.org/10.1016/j.ymeth.2017.06.025
668 Yao, R.-W., Luan, P.-F., Chen, L.-L., 2021. An optimized fixation method containing glyoxal
669 and paraformaldehyde for imaging nuclear bodies. RNA 27, 725–733.
670 https://doi.org/10.1261/rna.078671.120
671 You, S., Yu, A.M., Roberts, M.A., Joseph, I.J., Jackson, F.R., 2021. Circadian regulation of the
672 Drosophila astrocyte transcriptome. PLoS Genet 17, e1009790.
673 https://doi.org/10.1371/journal.pgen.1009790
674 Young, S.K., Wek, R.C., 2016. Upstream Open Reading Frames Differentially Regulate Gene-
675 specific Translation in the Integrated Stress Response. Journal of Biological Chemistry
676 291, 16927–16935. https://doi.org/10.1074/jbc.R116.733899

677 Yu, H.-H., Awasaki, T., Schroeder, M.D., Long, F., Yang, J.S., He, Y., Ding, P., Kao, J.-C., Wu,
678 G.Y.-Y., Peng, H., Myers, G., Lee, T., 2013. Clonal Development and Organization of
679 the Adult Drosophila Central Brain. Current Biology 23, 633–643.
680 https://doi.org/10.1016/j.cub.2013.02.057
681 Zhang, H., Dou, S., He, F., Luo, J., Wei, L., Lu, J., 2018. Genome-wide maps of ribosomal
682 occupancy provide insights into adaptive evolution and regulatory roles of uORFs
683 during Drosophila development. PLoS Biol 16, e2003903.
684 https://doi.org/10.1371/journal.pbio.2003903
685 Zhang, H., Wang, Y., Lu, J., 2019. Function and Evolution of Upstream ORFs in Eukaryotes.
686 Trends in Biochemical Sciences 44, 782–794.
687 https://doi.org/10.1016/j.tibs.2019.03.002
688 Zuker, C.S., Cowman, A.F., Rubin, G.M., 1985. Isolation and structure of a rhodopsin gene
689 from D. melanogaster. Cell 40, 851–858. https://doi.org/10.1016/0092-
690 8674(85)90344-7
691
692

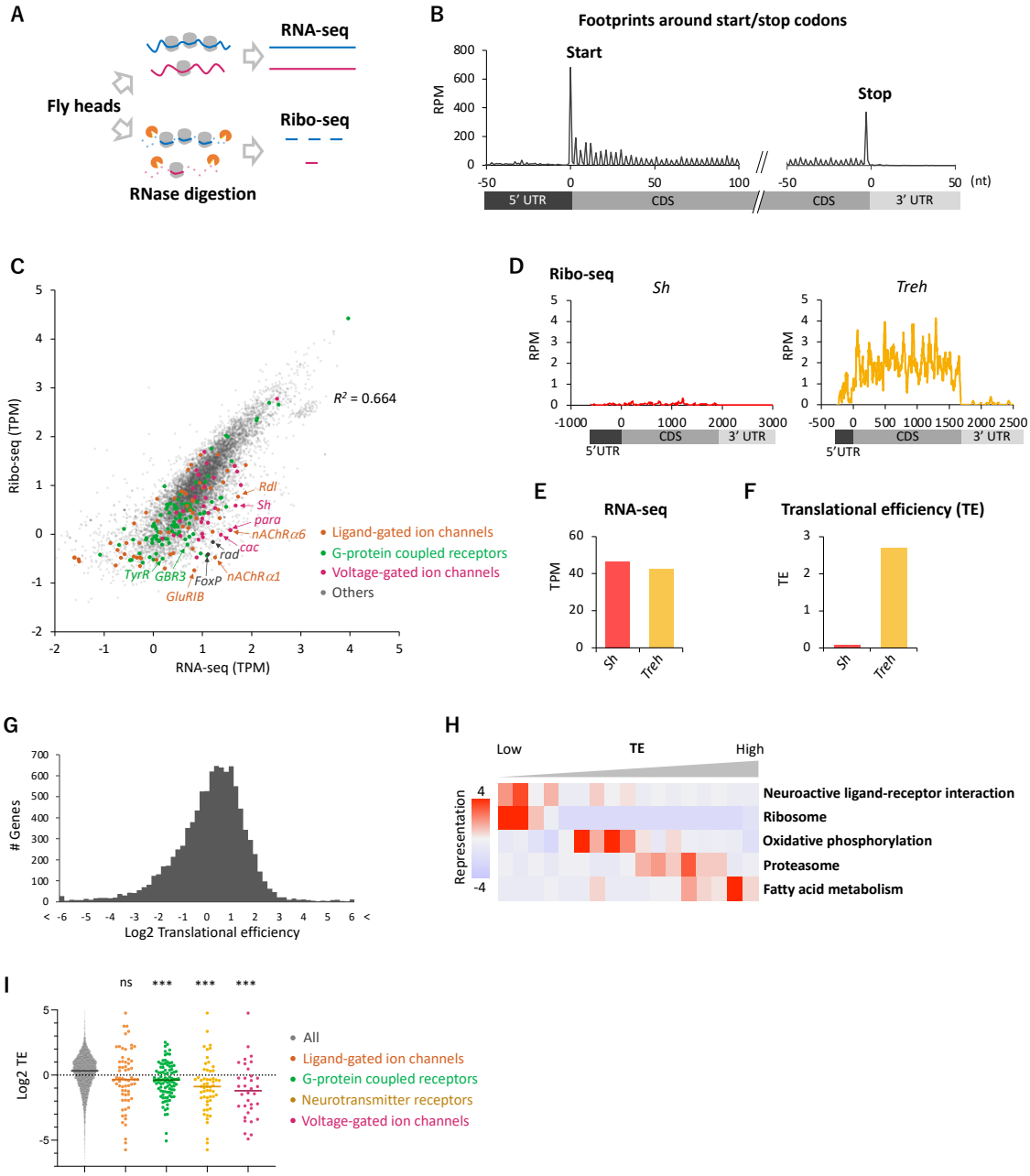

Figure 1. Comparative transcriptome-translatome analyses in the *Drosophila* head.

(A) Schematics. Fly head lysate is digested with RNase I for Ribo-seq, while not for RNA-seq. Resultant short fragments or the whole mRNA are reverse-transcribed and sequenced. (B) Meta-genome ribosome distribution (estimated P-sites of the 21-nt fragments), relative to the annotated start and stop codons. RPM: reads per million. (C) Scatter plots of mRNA reads (x-axis, TPM: transcripts per million) and ribosome footprints on CDS (y-axis, TPM). Several neuron-related genes are highlighted with colors and arrows. The squared Pearson's

701 correlation coefficient (R^2) is indicated. (D-F) Ribosome footprints (D), mRNA level (E), and
702 translational efficiency (F) of *Shaker-RB* (*Sh*) and *Trehalase-RA* (*Treh*). TE: translational
703 efficiency. TE is calculated as ribosome footprints on CDS (TPM) divided by the mRNA level
704 (TPM). (G) Histogram of TE. The bin size is 0.2 in the unit of log 2. Total 9,611 genes with at
705 least one read in both Ribo-seq and RNA-seq are plotted. (H) Kyoto Encyclopedia of Genes
706 and Genomes (KEGG) pathways enrichment analysis, visualized by iPAGE (Goodarzi et al.,
707 2009), based on TE. The 9,611 genes are ranked and binned according to TE (left to right: low
708 to high), and over- and under- representation is tested. The presented KEGG pathways show
709 P values smaller than 0.0005. (I) TE of transcripts in the denoted gene ontology terms. Bars
710 represent the median. ns: $P > 0.05$; ***: $P < 0.001$; in the Dunn's multiple comparisons test,
711 compared to the "all" group.

712

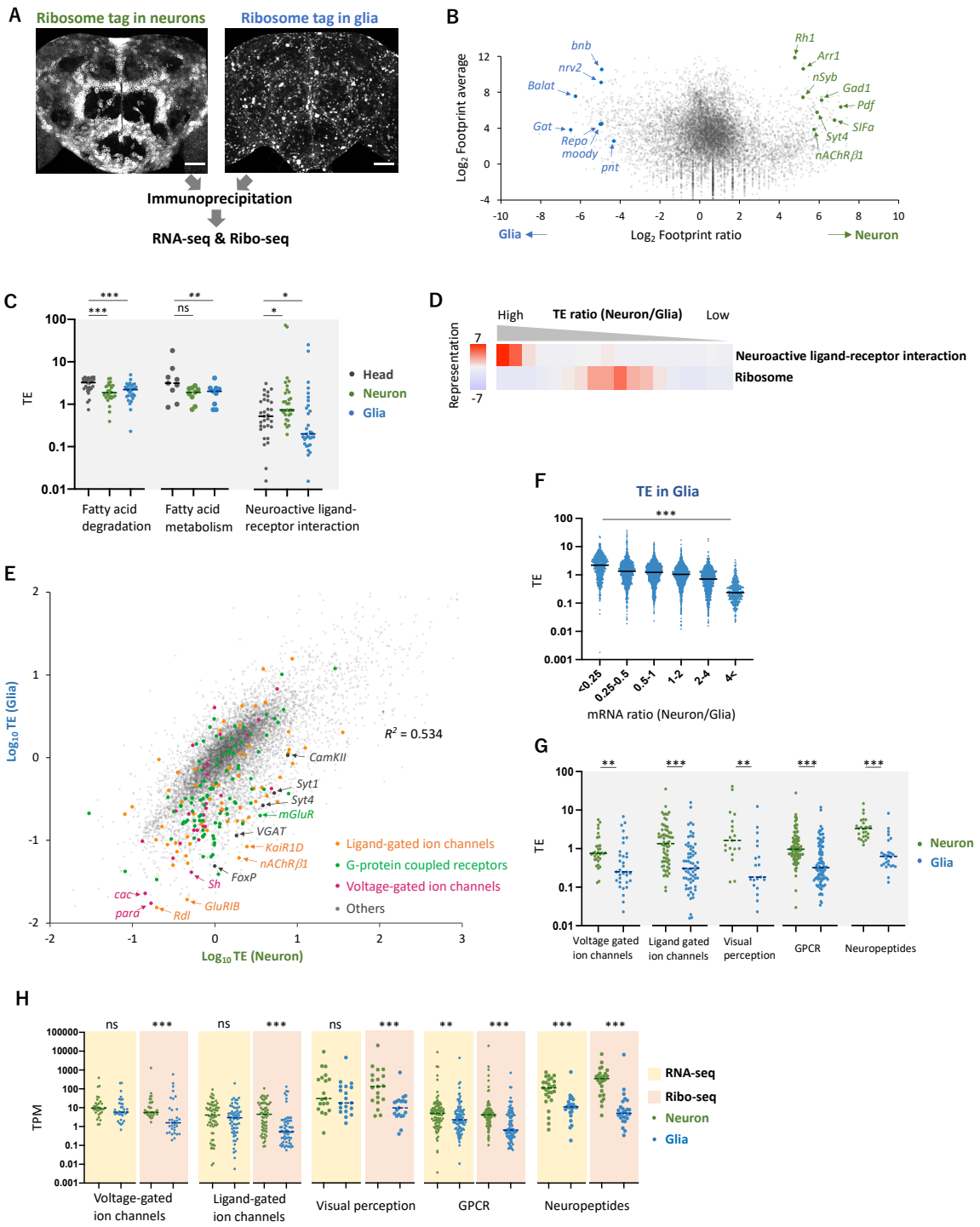

Figure 2. Cell-type specific Ribo-seq and RNA-seq reveal differential translational regulations.

(A) Schematics. FLAG-tagged ribosome protein L3 (RpL3::FLAG) is expressed in neurons (*nSyb-GAL4*) or in glial cells (*repo-GAL4*). RNA-seq and ribo-seq are performed following

718 immunoprecipitation. Whole brain images of the exogenously expressed RpL3::FLAG are
719 shown. Scale bars: 50 μm. (B) The MA-plot of ribosome footprints on CDS among neurons
720 and glia. Each gene is plotted according to the fold change (x-axis) and the average (y-axis)
721 in the unit of $\log_2$. Several marker genes are highlighted with green (neuron) or blue (glia). (C)
722 TE of genes in the denoted KEGG pathways in the whole head (black), neurons (green), or in
723 glia (blue). Genes with TPM > 1 in the RNA-seq dataset are plotted. Bars represent the
724 median. *: $P < 0.05$, **: $P < 0.01$, ***: $P < 0.001$, the Dunn's multiple comparisons test. (D)
725 KEGG pathway enrichment analysis based on the ratio of TE in neurons to in glia. All genes
726 with at least one read in both cell types (total 9,732 genes) are ranked and binned according
727 to the neuron-to-glia ratio (left to right: high to low), and over- and under- representation is
728 tested. The presented KEGG pathways show *P* values smaller than 0.0005. (E) Scatter plot of
729 TE in neurons (x-axis) and in glia (y-axis). The squared Pearson's correlation coefficient (R^2)
730 is indicated. (F) TE in glia plotted according to the ratio of mRNA expression in neurons
731 compared to glia. ***: $P < 0.001$, Kruskal-Wallis test. (G) TE of transcripts in the indicated gene
732 ontology (GO) terms. Bars represent the median. **: $P < 0.01$, ***: $P < 0.001$, Mann-Whitney
733 test of ranks. (H) Read counts of genes (TPM) in the indicated GO terms in RNA-seq (yellow)
734 and in ribo-seq (pink). The green and blue dots indicate the read counts in neuronal and glial
735 cells, respectively. ns: $P > 0.05$, **: $P < 0.01$, ***: $P < 0.001$, Mann-Whitney test of ranks.
736

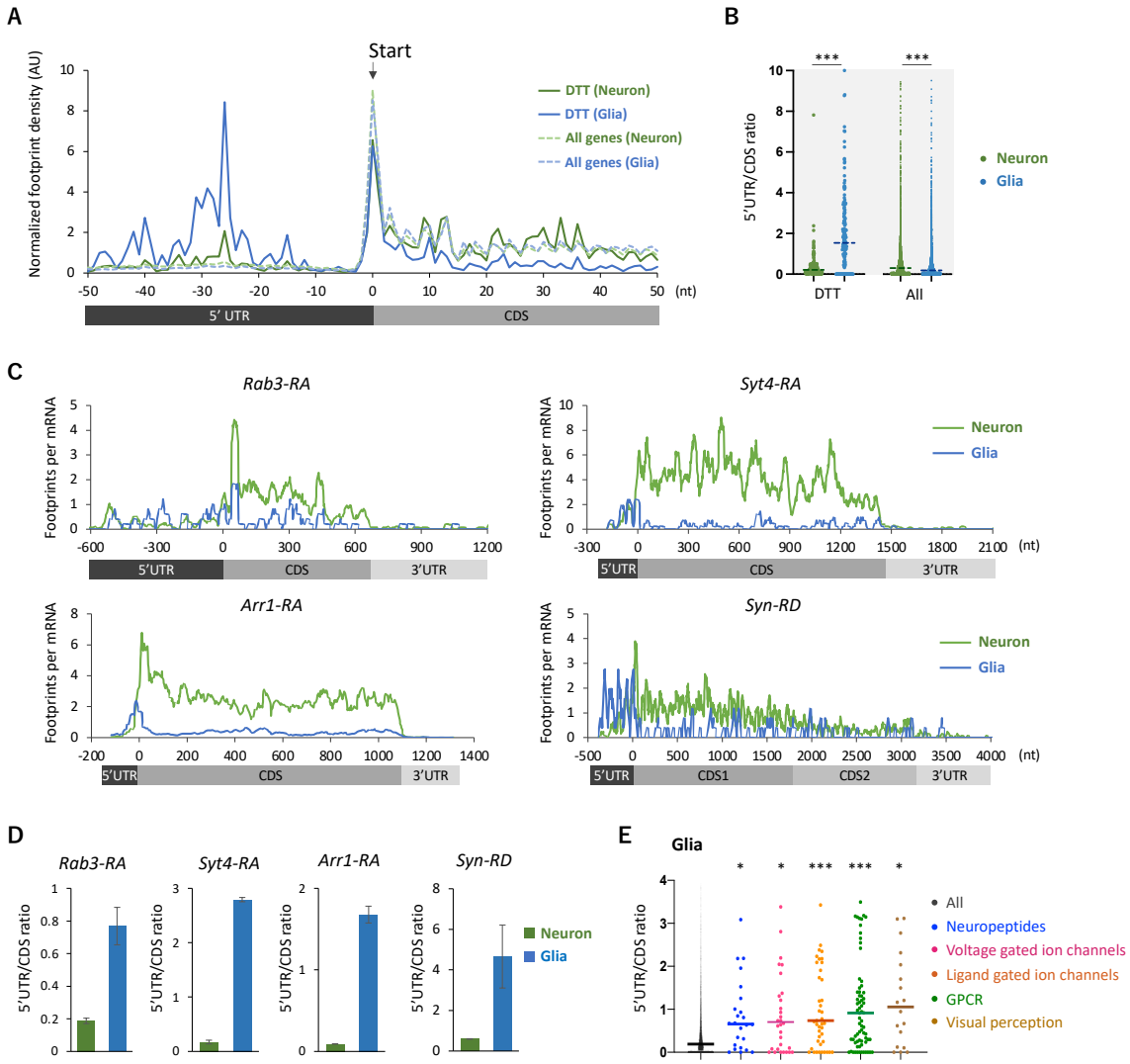

Figure 3. Ribosome stalling on the 5′ UTR of DTTs in glia.

(A) Ribosome distribution (estimated P-sites) on the 161 DTTs around the start codons (solid lines; start +/- 50 nt). These DTTs are defined as transcripts showing more than 10 times higher TE in neurons compared to glia. The dotted lines indicate the genome-wide distribution. Only transcripts showing TPM > 1 in RNA-seq both in neurons and glia are considered (7,933 genes in total), and the height is normalized by the total reads on this region. (B) Ratio of ribosome density on 5′ UTR (TPM) to CDS (TPM) of the 161 DTTs or of all transcripts in neurons (green) or in glia (blue). The bars represent the median. ***: $P < 0.001$, Mann-Whitney test of ranks. (C) Distribution of ribosome footprints on the representative neuronal transcripts. Ribosome footprints (RPM) normalized by the mRNA level (TPM) are shown. Note that *Syn-RD* harbors a stop codon in the CDS but a fraction of ribosomes skip it, generating two

749 annotated ORFs (CDS1 and CDS2) (Klagges et al., 1996). (D) Ratio of ribosome density on
750 5′ UTR to CDS (mean ± standard error of mean of the biological replicates). (E) Ratio of
751 ribosome density on 5′ UTR to CDS on transcripts in the indicated GO terms in glia. *: $P <$
752 0.05, ***: $P < 0.001$, Dunn's multiple comparisons test compared to the "all" group.
753

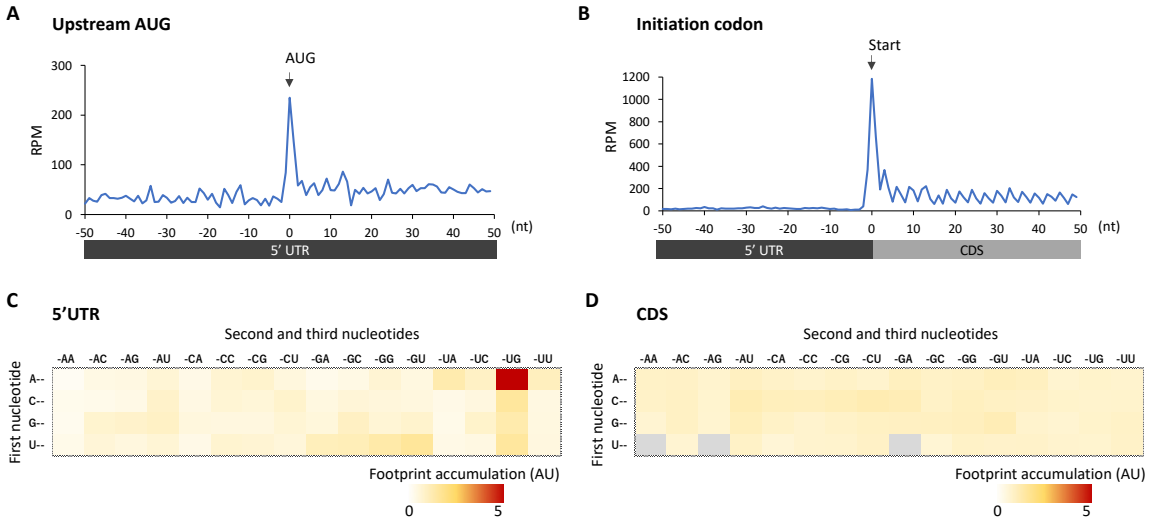

Figure 4. Footprint accumulation on upstream AUG in glia.

(A) Meta-genome ribosome distribution (estimated P-sites of the 32-nt fragments) around the upstream AUG codons in glia. (B) Meta-genome ribosome distribution (estimated P-sites of the 32-nt fragments) around the annotated start codons in glia. (C) Footprint accumulation on 5′ UTR in glia, defined as the number of ribosome footprints (estimated P-sites) on each codon normalized by the average on the surrounding (-50 to +50) regions. (D) Footprint accumulation inside the annotated CDS in glia. Annotated in-frame codons except the start and the stop codons are considered. AU: arbitrary unit.

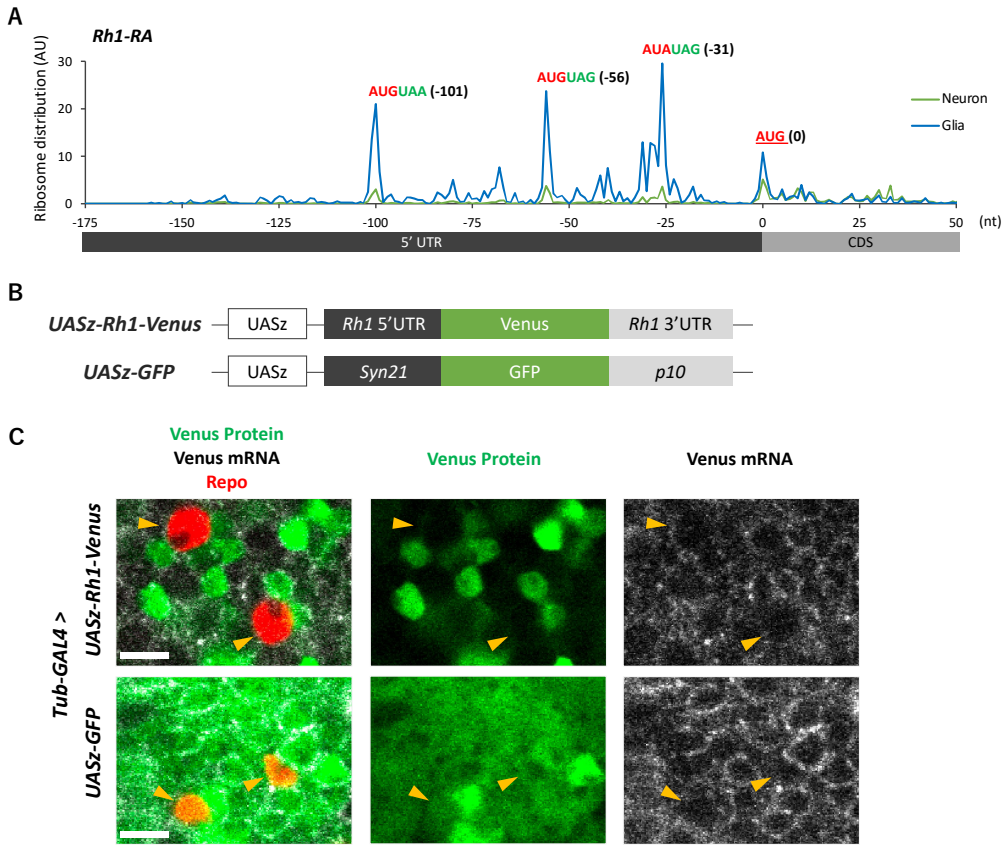

Figure 5. The transgenic *Rh1-Venus* reporter reveals differential translation in neuronal and glial cells.

(A) Ribosome distribution (estimated P-sites) on *Rh1-RA* in neurons (green) and in glia (blue), with 0 on the x-axis indicating the start codon of the CDS. 6-base upstream ORFs, consisting of consecutive start (or the near-cognate) and stop codons, are highlighted. Footprints are normalized by the total read counts on the transcript in each cell type. (B) Schematics of the *Rh1* (*UASz-Rh1-Venus*) or the control (*UASz-GFP*) reporter. For the *Rh1* reporter, 5' UTR and 3' UTR sequences of *Rh1-RA* are fused to CDS of the *Venus* fluorescent protein. For the control reporter, synthetic 5' UTR sequences (*syn21*) and viral *p10* terminator are fused to GFP (DeLuca and Spradling, 2018). Note that both reporters contain the same promoter (*UASz*) (DeLuca and Spradling, 2018) and are inserted onto the identical genomic locus (*attP40*). (C) Expression of the *Rh1*- or the control reporters driven by *Tubulin-GAL4*. Sliced confocal images of the cortical regions next to the antennal lobe are shown. Green: EGFP or Venus fluorescent signal. Red: Immunohistochemical signal of repo protein as a glial marker. Grey: EGFP or Venus mRNA. Orange arrowheads indicate glial cells marked by the repo expression. Scale bars: 5 μm.